JOURNAL OF MATERIALS SCIENCE 28 (1993) 1532–1536

An effect of microstructure on the interface resistance between a perovskite-type oxide electrode and yttria-stabilized zirconia

TAKANORI INOUE, KEIICHIRO HOASHI, KOICHI EGUCHI, HIROMICHI ARAI*
Department of Materials Science and Technology, Graduate School of Engineering Sciences, Kyushu University, 6-1 Kasugakoen, Kasuga-shi, Fukuoka 816, Japan

The electrode characteristics of perovskite-type oxides, $La_{0.6}Sr_{0.4}CoO_3$ and $La_{0.6}Sr_{0.4}MnO_3$, on ceria-based oxide and stabilized zirconia were analysed by the a.c. impedance method. The ionic conductivities of the electrolyte and electrode conductivities from the a.c. impedance analysis agreed with those obtained from the current interruption and d.c. four-probe methods. Two semicircles from the charge transfer and diffusion processes appeared as the electrode resistance. The relative contribution of these two processes to the overall electrode resistance strongly depended on the microstructure of the electrode. The electrode microstructure could be controlled by the dispersion medium used for the electrode slurry. The $La_{0.6}Sr_{0.4}MnO_3$ electrode coated with n-butyl acetate slurry exhibited the smallest electrode resistance.

1. Introduction

The electrochemical properties of an oxygen concentration cell with an oxide electrolyte are strongly affected by the electrode materials, particularly when the cell is operated at low temperatures [1]. Perovskite-type oxides, such as the La–Sr–Co–O and La–Sr–Mn–O systems, have been known to possess excellent characteristics as electrodes for yttria-stabilized zirconia (YSZ) or ceria-based oxide solid electrolytes [2, 3]. We have reported that these perovskite-type oxide electrodes are effective in lowering the operating temperature of fuel cells and oxygen sensors due to their low cathodic overpotential [4]. The electrode reaction kinetics was discussed on the basis of polarization data obtained by the current interruption method [4–6]. Since the Co-based oxides become reactive to YSZ electrolyte at 1000 °C or higher, these electrodes are attractive for low-temperature applications of O_2 concentration cells [4, 7, 8].

The electrode reaction rate or electrode resistance is expected to be affected by the particle size of the electrode and the microstructure as well as the type of electrode material. In this paper, we report an investigation of the electrode resistance at the electrolyte–cathode interface by the a.c. impedance method and the current interruption method. The influence of the microstructure of electrode materials on the electrode–electrolyte interface resistance is discussed.

2. Experimental procedure

$(ZrO_2)_{0.92}(Y_2O_3)_{0.08}$ and $(CeO_2)_{0.8}(SmO_{1.5})_{0.2}$ were prepared by calcination of the component oxide mixtures. The oxide mixtures of calculated amounts of CeO_2 (99.9%) and Sm_2O_3 (99.9%) or ZrO_2 (99.9%) and Y_2O_3 (99.9%) were ball-milled for 24 h and then calcined at 1300 °C for 10 h. The calcined powder was pulverized and subsequently pressed into a disc (20 mm in diameter and 1.8 mm thick) at 2.0×10^8 Pa *in vacuo*. The pressed disc was sintered at 1650 °C for 15 h.

Perovskite-type oxides, $La_{0.6}Sr_{0.4}CoO_3$ and $La_{0.6}Sr_{0.4}MnO_3$, were prepared by pyrolysis of the corresponding metal acetates and solid-state reaction at 900 °C. The powder of perovskite-type oxide was mixed with dispersion media, i.e. methyl cellulose, turpentine oil, n-butyl acetate and water, as listed in Table I. The slurry thus obtained was applied to both sides of the solid electrolyte disc and used as the working and counter electrodes. A platinum reference electrode (KT-5, Tanaka Matthey) was also placed on the electrolyte disc. The disc was calcined at 1000 to 1200 °C for 1 h after applying the electrode. The electrodes prepared from different dispersion media are expressed hereafter by symbols as listed in Table I.

The following oxygen concentration cell was studied:

$$O_2 + N_2(P_{O_2}), \text{ electrode/electrolyte/electrode, } O_2 + N_2(P_{O_2})$$

where the electrode was $La_{0.6}Sr_{0.4}MnO_3$ or $La_{0.6}Sr_{0.4}CoO_3$ and the electrolyte $(ZrO_2)_{0.92}(Y_2O_3)_{0.08}$ or $(CeO_2)_{0.8}(SmO_{1.5})_{0.2}$. The partial pressure of oxygen (P_{O_2}) was controlled from 10^5 to 1 Pa at 600–1000 °C. The electrolyte and electrode resistances were estimated from the a.c. impedance method using an impedance meter (NF Electronic Instruments, S-5720C) in the frequency range of 100 mHz–100 kHz. The applied voltage, V_{p-p}, was

*Author to whom all correspondence should be addressed.

0022–2461

TABLE I $La_{0.6}Sr_{0.4}MnO_3$ electrodes used in the present study

Electrode	Dispersion medium	Firing temperature (°C)
LSM-M-T	Methyl cellulose + turpentine oil	1000
LSM-T	Turpentine oil	1000
LSM-N	n-butyl acetate	1000
LSM-W-1000	Water	1000
LSM-W-1100	Water	1100
LSM-W-1200	Water	1200

Every electrode was prepared from a slurry of $La_{0.6}Sr_{0.4}MnO_3$ powder and a dispersion medium.

kept less than 10 mV. The complex impedance was measured by the three-probe or two-probe method.

3. Results and discussion

3.1. The electrolyte and electrode resistance

The electrode and electrolyte resistances of the oxygen concentration cell with a $(CeO_2)_{0.8}(SmO_{1.5})_{0.2}$ electrolyte and $La_{0.6}Sr_{0.4}CoO_3$ electrode, mixed with turpentine oil and calcined at 1000 °C, are estimated from a.c. impedance analysis and the current interruption method. Fig. 1 shows Cole–Cole plots for the cell at 800 °C at three different values of P_{O_2}. Of the two intercepts of the arc, the resistance at the high-frequency intercept was unchanged with P_{O_2}, whereas the low-frequency intercept strongly depended upon P_{O_2}. The resistance at the high-frequency intercept is considered to be the electrolyte resistance. The ionic conductivity of the electrolyte, σ_i, was obtained from

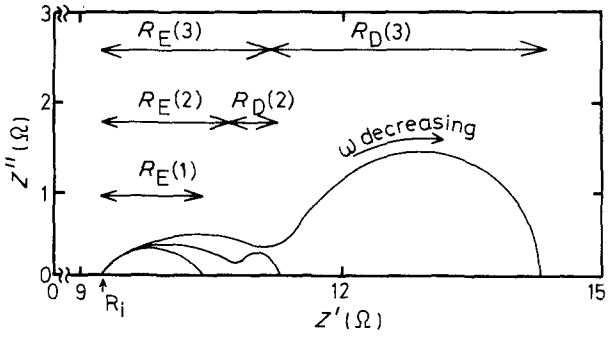

Figure 1 Cole–Cole plots for $La_{0.6}Sr_{0.4}CoO_3$ electrode on $(CeO_2)_{0.8}$ $(SmO_{1.5})_{0.2}$ electrolyte at 800 °C at (1) $P_{O_2} = 10^5$ Pa, (2) $P_{O_2} = 10^3$ Pa and (3) $P_{O_2} = 10^2$ Pa. R_i is the intercept on the Z' axis in the high-frequency region, R_E is calculated from the first arc and R_D from the second arc.

R_i as summarized in Table II from the equation

$$\sigma_i = l/R_iA \quad (1)$$

where A is the electrode area and l the electrolyte thickness. Table II also shows the ionic conductivities measured by the four-probe method and the current interruption method. In the latter method, the voltage drop was separated into the iR drop, which was simultaneously observed with the current interruption, and the overpotential η, which gradually decayed with time. The ionic conductivity was obtained from the iR drop because the iR drop corresponds to the ohmic component of the electrolyte. The ionic conductivities obtained from these three methods were very close. In the temperature range 600 to 1000 °C the arc for bulk and grain-boundary processes in the electrolyte appeared above a frequency of 100 kHz. Therefore, the resistance at the high-frequency intercept is attributed to the electrolyte resistance.

The shape and resistance of the semi-circular arcs strongly depended on P_{O_2}. This part of the resistance, i.e. R_E or $R_E + R_D$ in Fig. 1, is expected to be attributed to the electrode and/or electrode–electrolyte interface resistance. The impedance curves consisted of a single semicircular arc at high P_{O_2} but two arcs are obvious at low P_{O_2}. The electrode conductivities σ_E and σ_D were obtained from the two intercepts of the arc at the real axis (R_E and R_D) and from Equations 2 and 3 below after the two arcs were separated:

$$\sigma_E = 1/R_EA \quad (2)$$

$$\sigma_D = 1/R_DA \quad (3)$$

The σ_E values are summarized in Table II. The electrode conductivities measured by the current interruption method are also summarized in Table II. The electrode and/or electrode–electrolyte interface resistance, R_E, was obtained from the current density and the overpotential. The electrode conductivities from the a.c. impedance and the current interruption methods agreed with each other.

Fig. 2 shows the dependences of σ_E and σ_D on P_{O_2}. The σ_E value from the first arc exhibited a small dependence on P_{O_2} in the high P_{O_2} region, while its slope approached 1/4 in the low P_{O_2} region. It has been reported that the slope for σ_E is 1/4 when the charge transfer reaction is the rate determining step [4]. Of the two components in the electrode resistance, the first arc in the higher-frequency region is attributed to the chemical reaction and the second one in the lower-frequency region is the component with a

TABLE II Ionic conductivity of electrolyte, σ_i, and electrode conductivity, σ_E, at $P_{O_2} = 10^5$ Pa for $La_{0.6}Sr_{0.4}CoO_3/(CeO_2)_{0.8}P_{O_2}(SmO_{1.5})_{0.2}$ from the a.c. impedance, current interruption and d.c. four-probe methods

Temperature (°C)	A.c. impedance method		Current interruption		Four-probe method:
	σ_i (S cm^{-1})	σ_E (S cm^{-2})	σ_i (S cm^{-1})	σ_E (S cm^{-2})	σ_i (S cm^{-1})
600	1.07×10^{-2}	8.65×10^{-1}	1.16×10^{-2}	8.02×10^{-1}	1.29×10^{-2}
700	4.26×10^{-2}	3.17	3.77×10^{-2}	2.70	3.87×10^{-2}
800	8.53×10^{-2}	8.27	8.88×10^{-2}	7.87	9.02×10^{-2}

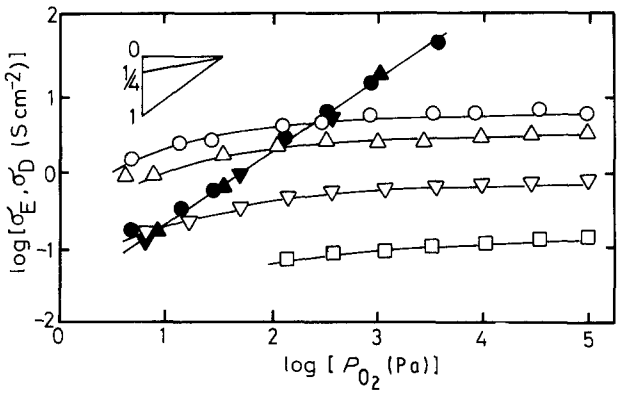

Figure 2 P_{O_2} dependence of $\log \sigma_E$ (open symbols) and $\log \sigma_D$ (closed symbols) for $La_{0.6}Sr_{0.4}CoO_3/(CeO_2)_{0.8}(SmO_{1.5})_{0.2}$ at (○,●) 800 °C, (△,▲) 700 °C, (▽,▼) 600 °C and (□) 500 °C.

larger time-constant. The second arc appeared only in the low P_{O_2} region, and the slope of σ_D against P_{O_2} was unity. Although σ_E decreased with decreasing temperature because the electrode reaction becomes slow, σ_D was unchanged with temperature. Tsuneyoshi *et al.* [9] have attributed σ_D to the diffusion process of oxygen molecules for the $La_{0.6}Sr_{0.4}MnO_3$ electrode. The σ_D component changes in proportion to P_{O_2} but is independent of temperature.

3.2 The particle size effect of electrode materials

As mentioned above, the a.c. impedance method is employed to separate the electrode resistance from the ohmic resistance of the electrolyte. An electrode reaction accompanies the diffusion of oxygen species in pores or on the surfaces of an electrode and reduction of oxygen to oxide ion around the three-phase boundary. The diffusion process and the length of the three-phase boundary are closely related with the microstructure and particle size of an electrode. In the present study, the effect of the microstructure of $La_{0.6}Sr_{0.4}MnO_3$ electrodes was investigated for cells with a $(ZrO_2)_{0.92}(Y_2O_3)_{0.08}$ electrolyte. It is found that the electrode microstructure can be easily modified by varying the kind of dispersion medium of the $La_{0.6}Sr_{0.4}MnO_3$ powder. Methyl cellulose, turpentine oil and water were used as dispersion media for the $La_{0.6}Sr_{0.4}MnO_3$ powder. The preparation conditions of electrodes are summarized in Table I. Fig. 3 shows the Cole–Cole plots of these cells at different P_{O_2} values.

Although only a single arc appeared at $P_{O_2} = 10^5$ Pa, the curve consisted of two arcs at $P_{O_2} = 10$ Pa for every LSM electrode. At $P_{O_2} = 10$ Pa, the second arc for the LSM-W-1000 electrode was larger than that for LSM-M-T and LSM-T electrodes. At intermediate P_{O_2} (10^2 Pa), the second arc was recognized only for the LSM-W-1000 electrode. Since the LSM-W-1000 electrode possesses a less porous microstructure than LSM-M-T and LSM-T electrodes, the second arc from the diffusion resistance of oxygen molecules is dominant at low P_{O_2}.

The electrode conductivities σ_E, at $P_{O_2} = 10^5$ Pa are plotted in Fig. 4 as a function of $1/T$. The LSM-N electrode exhibited the highest electrode conductivity among LSM electrodes. SEM photographs of the electrode materials are shown in Fig. 5. The LSM-M-T electrode was porous, whereas the LSM-W-1000 electrode was dense. Observation of SEM photographs indicated the following sequence of porosity of the electrode materials:

porous ← LSM-M-T electrode (methyl cellulose and turpentine oil)
> LSM-T electrode (turpentine oil)
> LSM-N electrode (n-butyl acetate)
> LSM-W-1000 electrode (water fired at 1000 °C) → dense

Microstructural models of the LSM electrodes are shown in Fig. 6. The electrode resistance is affected by the morphology of the electrode material, particularly by the length of the gas–electrode–electrolyte boundary. The LSM-W-1100 and LSM-W-1200 electrodes which were coated by using a water-based slurry consisted of very coarse particles. The particles appear to undergo grain growth with the aid of adsorbed water during the heating process. Methyl cellulose and turpentine oil decompose on heating, leaving a large content of voids in the electrode. Thus, the loosely packed microstructure gives rise to a small electrode–electrolyte interface area. The LSM-N elec-

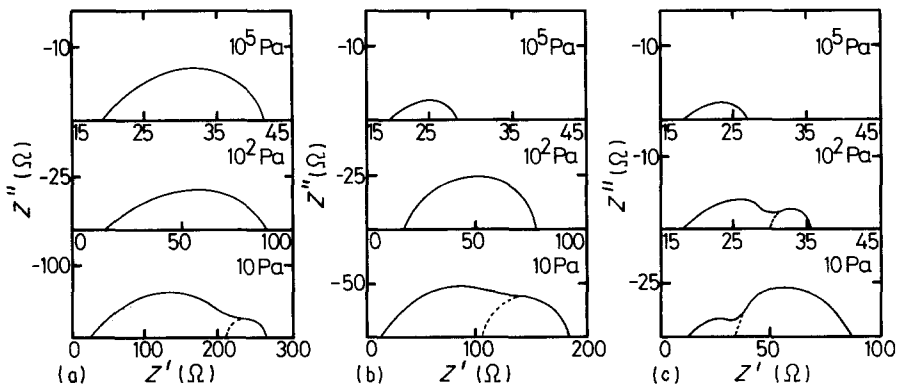

Figure 3 Cole–Cole plots of $La_{0.6}Sr_{0.4}MnO_3/(ZrO_2)_{0.92}(Y_2O_3)_{0.08}$ at 800 °C: (a) LSM-M-T, (b) LSM-T, (c) LSM-W—1000. Preparation conditions of every electrodes are shown in Table I. Pressures in the figure are P_{O_2}.

trode, coated by n-butyl acetate-based slurry, possesses a relatively large interface area and a long gas–electrode–electrolyte boundary, which contributes to the electrode reaction. Thus, this electrode exhibited the highest electrode conductivity. n-butyl acetate vaporizes at room temperature. The electrode consists of densely packed particles and contains a large number of micropores.

At $P_{O_2} = 10^2$ Pa, two arcs were recognized for the LSM-W-1000 electrode, because the electrode possesses a less porous microstructure. On the other hand, LSM-T and LSM-M-T electrodes possess a porous microstructure, so only one arc was recognized at $P_{O_2} = 10^2$ Pa. At $P_{O_2} = 10$ Pa, for the LSM–W–1000 electrode the second arc was larger than the first arc. The electrodes with less porous microstructure exhibited a high diffusion resistance at low P_{O_2}.

4. Conclusion

Perovskite-type oxides, $La_{0.6}Sr_{0.4}CoO_3$ and $La_{0.6}Sr_{0.4}$ MnO_3, were applied on ceria-based oxide and stabilized zirconia, and their electrode characteristics were analysed by the a.c. impedance method and the current interruption method. The microstructure of the perovskite electrode, and hence the preparation condition of the electrode, strongly affected the electrode resistance. The electrode resistance is found to

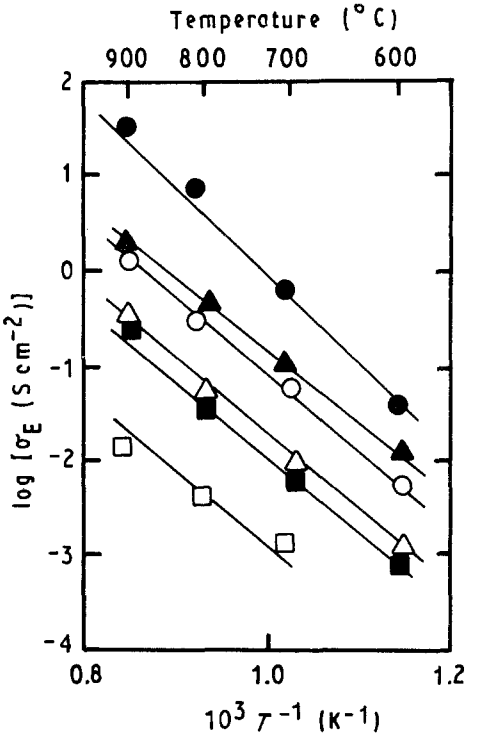

Figure 4 Arrhenius plots of electrode conductivity σ_E for $La_{0.6}Sr_{0.4}MnO_3/(ZrO_2)_{0.92}(Y_2O_3)_{0.08}$; $P_{O_2} = 10^5$ Pa. (△ LSM-M-T, (○) LSM-T, (●) LSM-N, (▲) LSM-W-1000, (■) LSM-W-1100, (□) LSM-W-1200. Preparation conditions of every electrode are listed in Table I.

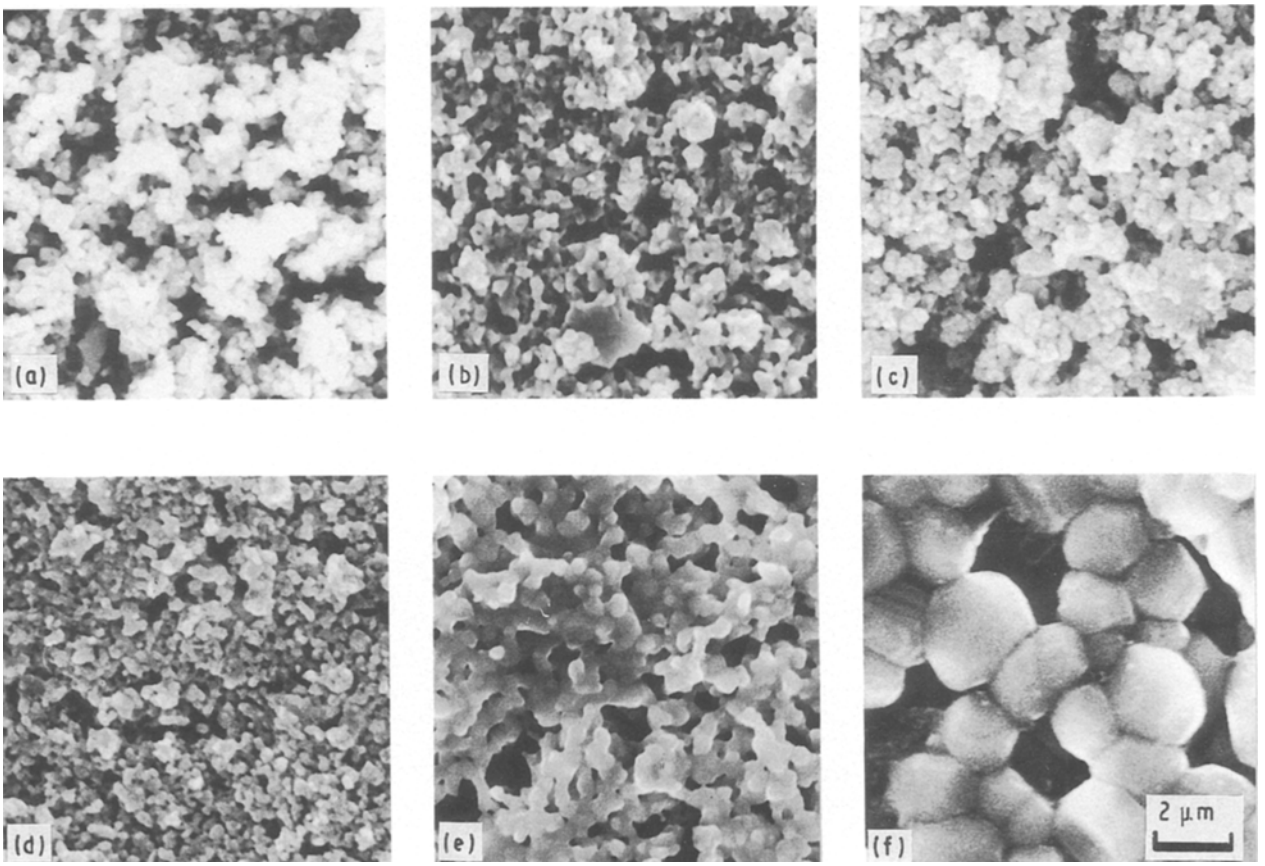

Figure 5 SEM images of surfaces of $La_{0.6}Sr_{0.4}MnO_3$ electrodes: (a) LSM-M-T, (b) LSM-T, (c) LSM-N, (d) LSM-W-1000, (e) LSM-W-1100, (f) LSM-W-1200. Preparation conditions of every electrode are listed in Table I.

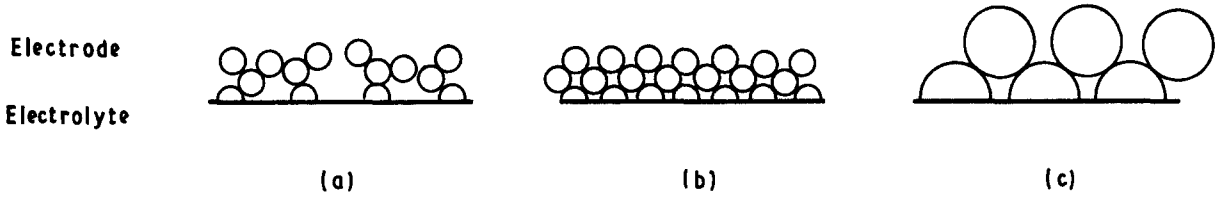

Figure 6 A schematic model of microstructures of the electrode–electrolyte interface. (a) LSM-M-T, mixed with methyl cellulose and turpentine oil and fired at 1000 °C; (b) LSM-N, mixed with n-butyl acetate and fired at 1000 °C; (c) LSM-W-1000, mixed with water fired at 1100 °C.

depend upon the kind of dispersion medium used for the electrode powder. In particular, the electrode applied on the electrolyte by using n-butyl acetate slurry exhibited the smallest electrode resistance. An effect of electrode microstructure is observed both on the charge transfer process and on the diffusion process during the electrode reaction.

References

1. T. INOUE, K. EGUCHI, T. SETOGUCHI and H. ARAI, *Solid State Ionics* **40/41** (1990) 407.
2. H. YAHIRO, Y. BABA, K. EGUCHI and H. ARAI, *J. Electrochem. Soc.* **135** (1988) 2077.
3. A. O. ISENBERG, *Solid State Ionics* **3/4** (1981) 431.
4. T.INOUE, N. SEKI, K. EGUCHI and H. ARAI, *J. Electrochem. Soc.* **137** (1990) 2523
5. DA YU WANG and A. S. NOWICK, *ibid.* **126** (1979) 1155.
6. J. MIZUSAKI, K. AMANO, S. YAMAUCHI and K. FUEKI, *Solid State Ionics* **22** (1988) 313.
7. Y. TAKEDA, R. KANNO, M. NODA, Y. TOMIDA and O. YAMAMOTO, *J. Electrochem. Soc.* **134** (1987) 2656.
8. N. SAKAI, T. KAWADA, H. YOKOKAWA and M. DOKIYA, *J. Mater. Sci.* **25** (1990) 4531
9. K. TSUNEYOSHI, K. MORI, A. SAWATA, J. MIZUSAKI and H. TAGAWA, *Solid State Ionics* **35** (1989) 263

Received 7 October 1991
and accepted 14 August 1992